Structural gradient based sizing optimization of wind turbine blades with fixed outer geometry

Sjølund, J. H.; Lund, E.

Published in:
Composite Structures

DOI (link to publication from Publisher):
10.1016/j.compstruct.2018.07.031

Publication date:
2018

Document Version
Accepted author manuscript, peer reviewed version

Paper A

Structural gradient based sizing optimization of wind turbine blades with fixed outer geometry

J. H. Sjølund, E. Lund

The paper has been published in
Composite Structures Vol. 203, pp. 725–739, 2018.
doi.org/10.1016/j.compstruct.2018.07.031

The layout has been revised.

Abstract

In this work the mass of a 73.5 m offshore wind turbine blade is minimized while considering manufacturing constraints, tip displacement, buckling, and static strength criteria when subject to an extreme load envelope consisting of 12 load directions. The gradient based sizing optimization takes offset in the outer geometry and loading from a commercial 73.5 m wind turbine blade where the manufacturing mold should be re-used and hence the outer geometry is kept constant. A solid-shell finite element model of the full blade is used as basis for the optimization. The blade is divided into patches and thicknesses of ply-groups (groups of contiguous plies with the same material and fiber orientation) are used as design variables. The design variables are assumed continuous in the optimization phase. Sequential linear programming (SLP) is used to solve the problem with semi-analytical gradients. In the post-processing phase the lay-up is refined and ply-group thicknesses are rounded to a whole number of plies. The gradient based sizing optimization results in a reduced mass and many active constraints across multiple load directions while the post-processing ensures manufacturability.

Keywords wind turbine blade structural design; gradient based sizing optimization; manufacturing constraints; laminated composites

A.1 Introduction

Modern wind turbine blades are complex composite structures. The blades are subject to complicated loading conditions and the materials have many different failure modes. The structure has a variable stiffness with ply-drops present throughout the blade. The ply-drops are accompanied by advanced material transitions between sandwich and monolithic sections, adhesive bonding, bolted connections, lightning protection and many other details. Modern wind turbine blades typically utilize either glass- or carbon-fiber reinforced polymers (GFRP/ CFRP), or even hybrids of these two, as the main load carrying materials. Wind turbine blades can be manufactured in many ways. One method is to place dry non-crimp fabric fiber mats in a mold, layer by layer. A mold exists for both the upwind (UW) side and the downwind (DW) side of the blade. The material is infused with resin in a vacuum-assisted process. Finally, the two halves of the blade are glued together with webs placed in-between. A typical cross section resulting from this process is illustrated in Figure A.1. The main laminate (MA), sometimes referred to as the spar cap, is mainly built from unidirectional (UD) layers. The trailing edge (TE) and leading edge (LE) are likewise reinforced by UD layers while core materials are usually covered by biaxial angle plies $\pm 45^{\circ}$. Basically, the main laminate carries the flapwise moment, trailing edge and leading edge laminates carry edgewise moments, sandwich panels in-between prevent local buckling, and the shear webs (SW) carry the shear load. The in-between sandwich panels are referred to as leading edge core (LEC) and trailing edge core (TEC) as shown in Figure A.1.

Structural optimization is often applied in the design of wind turbine blades. In this work the optimization is applied on an existing blade with the premise that the

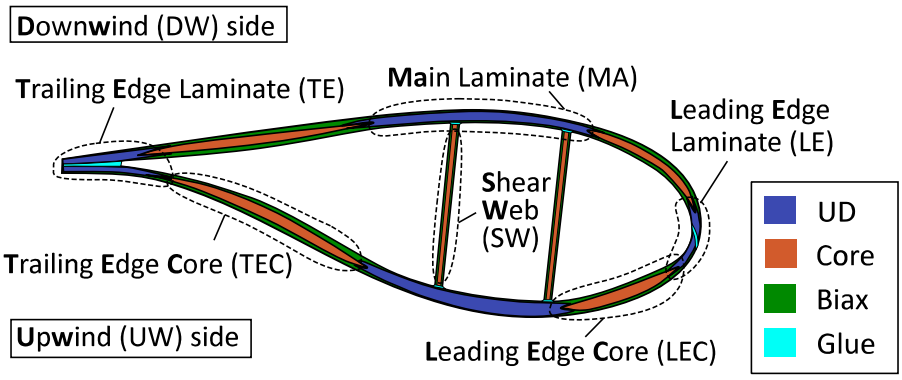

Fig. A.1: Typical wind turbine blade cross section.

manufacturing mold should be reused, and hence the outer geometry is considered fixed. Structural optimization of wind turbine blades with a fixed outer geometry has been investigated a number of times in the literature. The approaches taken can roughly be divided into two categories, the first being topology optimization where the optimal material distribution is sought, see e.g. Buckney et al. (2013) or Blasques and Stolpe (2012). This is usually without any a priori assumptions on blade build-up, but results are also often difficult to manufacture in practice. The other category is to utilize knowledge of typical blade build-up and limit the optimization to the sizing of the spanwise material distributions, the choice of material, and/or the position/size of members such as shear webs, spar cap etc. Here focus will be put on the second category. The spanwise sizing of materials is a discrete optimization problem as a manufacturable layup must consist of an integer number of plies at any point and only a discrete number of ply thicknesses is available.

In Jureczko et al. (2005), Chen et al. (2013), Barnes and Morozov (2016), and Bottasso et al. (2014) the optimization problem is relaxed by considering the sizing in terms of continuous thickness variables. Jureczko et al. (2005) use a layered shell finite element (FE) model to minimize the mass of a wind turbine blade. Two continuous thickness design variables are used for the sizing of shell and webs respectively. Constraints considered are stresses, tip displacement, and natural frequency. A genetic algorithm is used to solve the optimization problem. Chen et al. (2013) use a similar approach but instead take 9 material ply thicknesses as continuous design variables, hence changing a design variable corresponds to scaling the thickness of layers of the corresponding material throughout the blade. Barnes and Morozov (2016) consider the thickness of spar caps, shear webs skins and trailing edge reinforcement as continuous design variables along with a number of geometrical variables. The thicknesses are allowed to vary spanwise by dividing the blade into 6 stations longitudinally and the optimization problem is solved with a genetic algorithm. Bottasso et al. (2014) use a similar parameterization but includes leading edge reinforcement and skin core and uses 14 stations longitudinally. This results in 53 continuous thickness design variables and the problem is solved using a gradient based method. Furthermore, the optimization is separated in two loops. The gradient based optimization is done in the inner loop where a 2D cross-sectional FE model is used. The outer loop uses a finer 3D FE shell model which in turn calibrates the criteria used in the inner loop.

In Sørensen et al. (2014) and Albanesi et al. (2018) the wind turbine blade optimization problem is formulated such that a discrete number of plies is achieved. Sørensen et al. (2014) use a combined topology and multi-material approach on a ply basis to respectively determine whether or not there should be material and which material. Applied on a main spar with a patch parameterization and manufacturing constraints, this is solved using a gradient based method. In one case this method yields more than 30000 design variables. Albanesi et al. (2018) also use a multi-material approach, but in this case an empty ply is considered a material choice. The blade consists of a predetermined number of plies uniform over the cross section, and the design variables correspond to the material of each ply and the spanwise stopping position. Using 10 spanwise stations and 4 materials, this yields 121 design variables and the problem is solved by a genetic algorithm.

Modelling of wind turbine blades is typically done by layered shell 3D FE models. This is also the case in Jureczko et al. (2005); Albanesi et al. (2018), though Bottasso et al. Bottasso et al. (2014) also utilize a mixture of 3D and 2D solid FE models. Layered shell elements with an offset option are indeed very convenient to use since the outer geometry of a wind turbine blade is usually well defined. However, in some cases shell elements with offset have been found to introduce inaccuracies on torsional stiffness, see e.g. Laird et al. (2005) and Branner et al. (2007). In solid-shell elements the complications of element offset is avoided. Haselbach (2017) furthermore investigated trailing edge modelling in with the conclusion that a combined shell/solid model works well while a pure shell model does not predict the trailing edge stiffness correctly. Another advantage of solid-shell models is the possibility of a layer-wise refinement that allows insertion of e.g. cohesive zone elements to investigate delamination. In practice modern solid-shell elements (see e.g. ANSYS' SOLSH190 (ANSYS Inc., 2017) or the new ABAQUS element CSS8 (Dassault Systèmes, 2017)) can be used with no or little extra computational cost when compared to standard shell elements.

There are multiple objectives of this work. First of all the goal is to demonstrate the use of structural gradient based sizing optimization for the sizing of a modern 73.5 m offshore wind turbine blade using a full-scale 3D solid-shell finite element model. Next it will also be shown how knowledge on the typical build-up of wind turbine blades can be used to efficiently parameterize the blade with relatively few design variables while still including important manufacturing constraints. Furthermore, it will be demonstrated how including multiple constraint types and an extreme load envelope with 12 load directions will affect the spanwise material distribution in the different regions of the blade. Finally, it will be shown how sizing optimization using layered solid-shell can be performed as it involves both changing layup definition but also moving nodes like in shape optimization.

The paper is organized as follows: First the wind turbine blade along with parameterization, finite element model, loads, and criteria are presented in Section A.2. The optimization approach, shape design sensitivity, solution strategy, and post-processing are presented in Section A.3. Results from the optimization and post-processing are presented and discussed in Section A.4. Limitations of the approach are discussed in Section A.5 and the overall conclusion is presented in Section A.6.

A.2 Wind turbine blade

A.2.1 Blade description

This work takes offset in the outer geometry of a commercial 73.5 m offshore wind turbine blade. The outer geometry of the wind turbine blade is shown in Figure A.2. The blade is mainly built using GFRP with balsa as core material. Manufacturing is done with separate molds for upwind and downwind sides, and the infusion process uses polyester as resin. As mentioned in Section A.1 a typical cross section resulting from this process can be seen in Figure A.1. The blade has two standard shear webs spanning root to tip, and a third shear web near the trailing edge starting at 14 m and ending at 30 m when measured from the root. The wind turbine blade is divided into a number of characteristic regions: leading edge (LE), trailing edge (TE), main laminate (MA), leading edge core (LEC), and trailing edge core (TEC), corresponding to the colors in Figure A.2. Due to manufacturing the MA, TE, and LE regions have a constant width, and the LEC/TEC regions basically fill the space in-between. In this work widths of MA, TE, and LE are taken as 1200 mm, 800 mm, and 200 mm respectively.

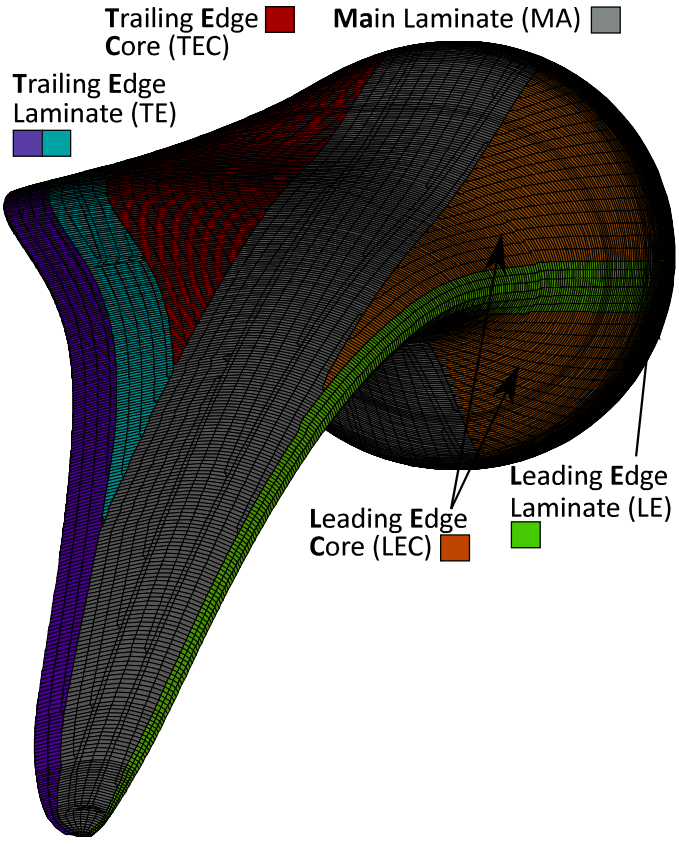

Fig. A.2: The outer geometry and finite element mesh of the 73.5 m offshore wind turbine blade. Colors correspond to the characteristic regions: Purple/blue is trailing edge (TE) with purple being the glue width, red is trailing edge core (TEC), gray is main laminate (MA), orange is leading edge core (LEC), and green is leading edge (LE).

A.2.2 Layup and parameterization

Cross-sectional parameterization

Assuming constant layup within the characteristic regions at a given spanwise position, and furthermore allowing the upwind and downwind parts to vary independently, a cross-sectional parameterization as shown in Figure A.3 is achieved. This assumption neglects details in the transitions between regions, but this can be accepted for a preliminary sizing. As part of the parameterization, contiguous plies of the same material and same orientation are grouped together in ply-groups. In doing so the layup of a given region can be defined through a sequence of ply-groups. The sequence of ply-groups for the TE region becomes biax-UD-biax as shown in Figure A.3. The number of plies in each of the ply-groups depends on the spanwise position in the blade, however the sequence is fixed. A ply-group can either be limited to a particular region, or it can span the entire cross section. The concept of ply-groups is particularly relevant for wind turbine blades where it is common to have many contiguous plies of the same material/orientation as opposed to the aircraft industry.

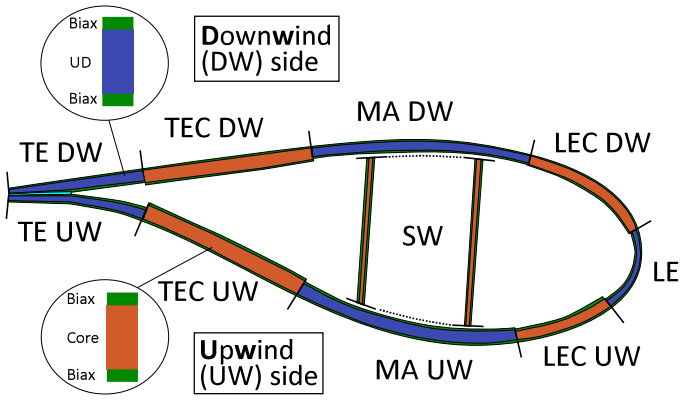

Fig. A.3: Cross-sectional parameterization with 10 characteristic regions. It also illustrates the constant layup within regions and the concept of ply-groups.

Longitudinal parameterization

The ply-groups should naturally be allowed to vary in thickness throughout the blade length. In this work the blade is divided into 2 m sections as shown in Figure A.4. In these sections the ply-groups have constant thickness. In practice a change in thickness is achieved with a ply-drop. Usually only one ply is allowed to be dropped at a time and the minimum distance between two ply-drops is limited. Here the limit is taken to 200 mm, i.e. 5 ply-drops per meter. Instead of letting the minimum ply-drop distance dictate the longitudinal discretization, the constraint is taken into account in an average sense as an allowed thickness change per unit length. This can be formulated as two linear constraints per ply-drop. As an example, the averaged ply-drop limit between patch p and adjacent patch $p+1$ in the main laminate layer l

can be written as:

$$t_{pl} - t_{(p+1)l} \leq S \tag{A.1}$$

$$t_{(p+1)l} - t_{pl} \leq S \tag{A.2}$$

where S is the allowed thickness change between the two patches. The allowed thickness change is the product of the allowed thickness change per meter, here corresponding to $5t^{\text{ply}}$/ m, and the patch length (2 m), where t^{ply} is the ply-thickness.

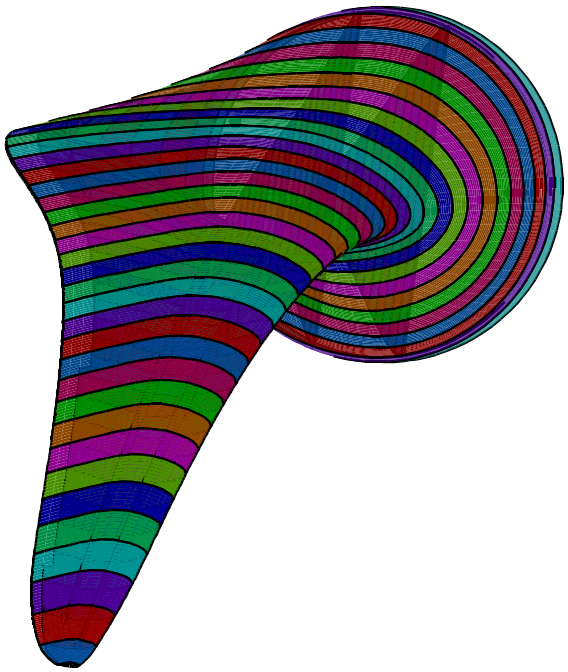

Fig. A.4: Longitudinal parameterization of wind turbine blade. The blade is divided into 2 m sections.

Layup and materials

A simplified layup utilizing only GFRP and balsa is defined through a sequence of ply-groups in Table A.1. The GFRP is infused with polyester and is assumed available as either UD or biaxial angle plies $\pm 45°$, here simply called biax. The first sequence number corresponds to the first layer placed in the mold which becomes the outer layer. The circumferential restriction refers to the regions in the cross section as shown in Figure A.1. The ply-groups that are not design variables have a constant number of layers as given in Table A.1. The design variable ply-groups have more complicated spanwise material distributions inspired by the distributions found in modern wind turbine blades and are scaled to provide a feasible starting point for optimization. The initial spanwise distributions for these ply-groups are shown later in the results section. As a starting point the upwind and downwind parts have identical layups, while they are allowed to vary independently in the optimization. Stiffness properties of GFRP-polyester are close to typical values with fiber volume fractions

of approximately 55%, and for the balsa close to typical values for densities of 150 kg/m^3.

Outer shell

Sequence no.	Ply-group name	Circumferential restriction	Design variable	Comment
1	Gelcoat	All over	No	Surface protection layer of 0.6 mm covering the whole blade (outer surface).
2	Biax	All over	No	4 layers of biax covering whole blade.
3	Root biax	All over	No	Additional 8 layers of biax near the root.
4	Root UD	All over	Yes	UD layers (all-over) near the root to distribute bolt loading and provide thickness for bolt inserts.
5	MA UD	MA	Yes	UD ply-group in the MA region.
6	LE UD	LE	Yes	UD ply-group in the LE region.
7	TE UD	TE	Yes	UD ply-group in the TE region.
8	LEC balsa	LEC	Yes	Balsa as core in the LEC region.
9	TEC balsa	TEC	Yes	Balsa as core in the TEC region.
10	Biax	All over	No	4 layers of biax covering whole blade (inner surface).
11	Glue	TE	No	Glue in the trailing edge.

Shear webs

Sequence no.	Ply-group name	Circumferential restriction	Design variable	Comment
1	Biax	SW	No	6 layers of biax as sandwich flange.
2	Balsa	SW	Yes	Balsa as core material.
3	Biax	SW	No	6 layers of biax as sandwich flange.

Table A.1: Layup of the wind turbine blade in terms of a sequence of ply-groups. The circumferential restriction either limits a ply-group to a specific region or span the entire cross-section. Ply-groups that are design variables have given initial spanwise distributions shown later in the results section.

A.2.3 Modelling strategy

A finite element model using layered solid-shell elements with one element through-the-thickness is used. The mesh is shown in Figure A.2 and consists of 27915 elements and 53808 nodes and is generated using a MATLAB program that takes airfoil geometry and layup as input. The internal mesh 21 m from the root can be seen in Figure A.5. The 3rd shear web mentioned earlier can also be seen. The mesh size is a compromise between accuracy and computational time, and is particularly important in optimization as the model is solved hundreds of times. Sufficient accuracy is verified according to GL (2010) which states that the lowest buckling eigenvalue must not change by more than 5% if the number of elements is doubled.

The use of solid-shell elements results in a continuous inner surface. The continuous inner geometry is achieved by having transition nodes with a thickness corre-

sponding to the average of its neighboring layups as shown in Figure A.5. The trailing edge is modeled with a 2 mm thin layer of glue between the upwind- and downwind parts, as can be seen on the zoom. The layup near the glue region is considered fixed due to the constant outer geometry and glue thickness. Since solid-shell elements are used a change in thickness corresponds to not only changing the layup definition but also moving nodes. The procedure to move nodes is explained in Section A.3.2.

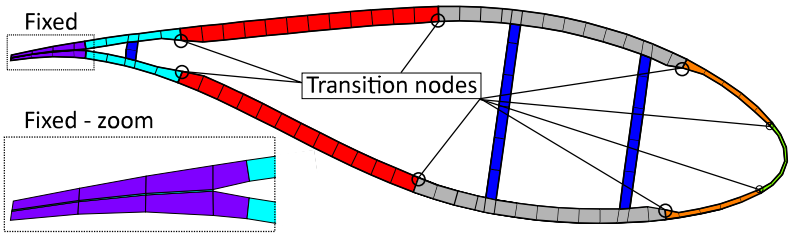

Fig. A.5: FE mesh shown at a cross section 21 m from root. Also shown is the transition nodes which have the average thickness of neighboring patches.

A.2.4 Completing the parameterization

Combining the cross-sectional and longitudinal parameterization results in a number of patches as shown in Figure A.6. Within the patches the layup is constant, though the transition nodes in-between patches are given the average thickness. Ply-groups have been introduced as a group of plies with same material and orientation. Determination of the optimal number of plies in a ply-group is a discrete optimization problem. In order to use gradient based methods, the problem is relaxed by considering the ply-group thicknesses as continuous design variables. To realize a manufacturable design after optimization the ply-group thicknesses are post-processed afterward as explained in Section A.3.4.

A.2.5 Loads

The loading of a wind turbine blade is comprised of many design load cases (DLC) corresponding to different loading situations. In this work an extreme load envelope based on IEC (2005) has been provided. The extreme load envelope consists of the maximum bending moments across all DLCs for multiple load directions. The load envelope contains 12 different load directions which is customary in the wind turbine industry. Less load directions can also be used but this is sometimes punished with higher partial safety factors, see e.g. DNV-GL (2015). The normalized load envelope is shown in Figure A.7 and the load directions are numbered from 1 to 12. The moments are normalized with respect to the positive flapwise bending moment (LC1) which deflects the blade towards the tower. The envelope is only visualized at the root, but each of the 12 load directions has a unique spanwise distribution which is fitted through 30 points using a cubic spline. In general, the ultimate limit state is taken as the characteristic loads multiplied with the partial factor $\gamma_f = 1.35$. Loading is applied to the FE model as surface pressure on the outer surface of the main laminate.

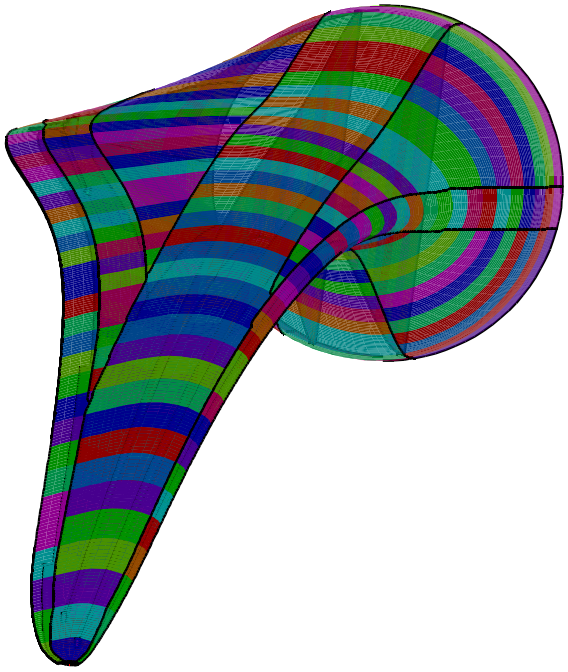

Fig. A.6: The resulting patches when combining the circumferential and longitudinal divisions of the blade. Ply-group thicknesses can vary independently in the patches as long as thickness variations are within the allowed limits.

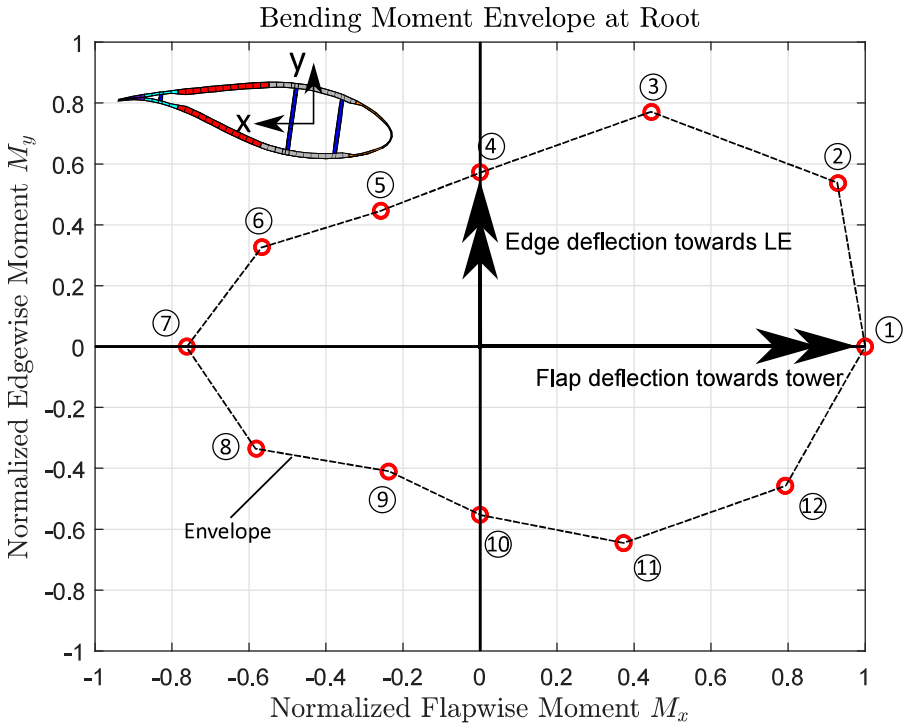

Fig. A.7: Static extreme design load envelope with 12 load direction here shown for the root. Envelope is normalized with the positive flapwise moment (load no. 1).

A.2.6 Design criteria

The wind turbine blade is to be designed according to a number of criteria from DNV-GL (2015). In this work criteria on tip displacement, short-term (static) strength, and buckling are considered. In practice wind turbine blade designs may also be governed by fatigue, adhesive joints, or natural frequencies. In the following demonstration the used criteria are chosen because they represent the overall problem types of displacements, eigenvalues, and local stresses and strains. Since the full 3D stress state is available when using solid-shell elements, strength criteria for adhesive joints can be included. Natural frequencies represent another eigenvalue problem and can also be considered. However, for simplicity adhesive joints and natural frequencies are not considered in the following demonstration. Including fatigue constraints in gradient based optimization is still an active area of research, and recent work by Oest and Lund (2017) on topology optimization using isotropic materials suggests that fatigue constraints can be included with similar computational costs as static stress/strain constraints. However, though very relevant, including fatigue constraints is left to future work.

Deflection

It must be verified that the wind turbine blade tip does not collide with the tower. In DNV-GL (2015) the allowed clearance depends on the tests performed and the monitoring available. In this work we disregard this and instead use a provided limit on the tip displacement of 18.5 m when the blade is subject to the extreme flapwise characteristic load, LC1.

Buckling

Buckling and stability are allowed to be verified in a number of ways DNV-GL (2015). In this work linear buckling FE analysis is performed by modelling the full blade and using 12 load directions. This yields the partial safety factors listed in Table A.2. The reduction factor γ_m for buckling becomes:

$$\gamma m_{buck} = \gamma_{m0} \cdot \gamma_{mc} \cdot \gamma_{m1} \cdot \gamma_{m2} \cdot \gamma_{m3} \cdot \gamma_{m4} \cdot \gamma_{m5} = 1.96 \tag{A.3}$$

The analyses are to be performed using the extreme load envelope based on ultimate limit state loads and for each of the 12 load directions the lowest buckling load factor should be larger than 1.96.

Short-term strength

Short-term strength is in DNV-GL (2015) divided into fiber failure (FF) and inter-fiber failure (IFF). For fiber failure the strains induced from design loads should be lower or equal to the design strain values. Design values are found by dividing characteristic values with a reduction factor. The reduction factor is based on the values listed in Table A.3 and is calculated as in equation A.3 resulting in $\gamma_{m_{FF}} = 2.41$.

In the case of inter-fiber failure Puck or Larc03 criteria should be used together with characteristic loads and a reduction factor $\gamma_{m_{IFF}} = 1.52$ again calculated using

Buckling

γ_{m0}	1.20	Base factor
γ_{mc}	1.08	For all analyses
γ_{m1}	1.05	Stiffness degradation
γ_{m2}	1.05	Temperature effects
γ_{m3}	1.10	Nominal material properties
γ_{m4}	1.25	Linear FE analysis
γ_{m5}	1.00	Load directions

Table A.2: Design resistance partial coefficients for buckling and stability.

Short-term strength

	FF	IFF	
γ_{m0}	1.20	1.20	Base factor
γ_{mc}	1.08	1.00	For all analyses
γ_{m1}	1.30	1.10	Long term degradation
γ_{m2}	1.10	1.00	Temperature effects
γ_{m3}	1.30	1.00	Manufacturing effects
γ_{m4}	1.00	1.15	Accuracy of method
γ_{m5}	1.00	1.00	Load directions

Table A.3: Design resistance partial coefficients for short-term strength in fiber failure (FF) and inter-fiber failure (IFF).

equation A.3 and Table A.3. In this work a maximum strain criterion is used instead for simplicity, and hence all transverse strength properties are divided by $\gamma_{m_{IFF}}$ and fiber-direction properties by $\gamma_{m_{FF}}$. Strength values are close to typical values for GFRP-polyester composites with fiber volume fractions of approximately 55%.

A.3 Optimization approach

A.3.1 Optimization problem

The optimization problem can be written as:

$$
\begin{array}{lllll}
\min\limits_{\mathbf{t}} & m & & & \text{(mass)} \\
\text{s.t.} & \lambda_n^{\mathrm{LC}} \geq 1.96, & \mathrm{LC} = 1 \ldots 12, \; n = 1 \ldots 8 & & \text{(buckling)} \\
& (\max \mathrm{FI})^{\mathrm{LC}} \leq 1.0, & \mathrm{LC} = 1 \ldots 12, & & \text{(failure index)} \\
& \left| u_{\mathrm{tip}}^{\mathrm{flap}} \right| \leq 18.5\mathrm{m} & & & \text{(displacement)} \\
& \text{ply-drop constraints} & & & \text{(manufacturing)} \\
& \underline{t_{pl}} \leq t_{pl} \leq \overline{t_{pl}} & & & \text{(design variables)}
\end{array}
$$

where m is the mass, $\mathbf{t}$ is a vector of design variables, λ_n^{LC} is linear buckling load factors, $u_{\text{tip}}^{\text{flap}}$ is the tip displacement in the flapwise load case, and FI is the failure index using the max. strain criterion. Buckling load factors and failure indices are evaluated for 12 load cases each (index LC), and for each buckling criterion the 8 lowest buckling load factors are found (index n) to take into account mode switching during the optimization. Design variable t_{pl} corresponds to the continuous ply-group thickness of layer l in patch p. There are a total of 406 design variables constrained by 678 ply-drop constraints in the optimization problem.

Failure indices are calculated for the top and bottom of each layer of each element in the model. If included directly in the optimization problem this yields a large number of constraints. In order to reduce this number a P-norm (PN) approach is used such that the maximum failure index is approximated as:

$$\text{FI}_{\text{PN}} = \left(\sum_{l=1}^{n_{\text{FI}}} (\text{FI}_l)^P \right)^{1/P} \tag{A.4}$$

In this work a P-norm is calculated for each patch and thereby the number of failure index values is reduced from approximately 1,022,000 to 353 (the number of patches). The number of failure indices, n_{FI}, within each patch varies according to the number of elements within the patch. The P parameter is a compromise between better approximations of the maximum value and numerical issues. Here a value of $P = 8$ is used and in each patch the 10 highest values are included in the P-norm. A P-norm will always overestimate the largest failure index. In order to avoid this overestimation an adaptive constraint scaling scheme is used, see Oest and Lund (2017) for details. The P-norm approach applied is described in more detail in Lund (2018).

A.3.2 Finite element analysis and sensitivities

Finite element analysis and design sensitivity analysis is performed using an in-house research code written in Fortran 95. The framework is called MUltidisciplinary Synthesis Tool (MUST), see MUST (2018) for more information. In this work solid-shell finite elements are used. The solid-shell implementation utilizes assumed natural strain (ANS) and enhanced assumed strain (EAS) formulations to avoid various locking phenomena. The element formulation is described in more detail in Johansen and Lund (2009).

Analysis

The element stiffness matrix for element e can be written as:

$$\mathbf{K}^e = \sum_{l=1}^{n_l} \int (\mathbf{B}_l^e)^T \mathbf{C}_l^e \mathbf{B}_l^e dV \tag{A.5}$$

where l is the layer number, n_l is the number of layers, $\mathbf{B}_l^e$ is the layer strain-displacement matrix, and $\mathbf{C}_l^e$ is the layer constitutive matrix. The global stiffness matrix $\mathbf{K}$ is assembled from the individual element stiffness matrices. The governing equation for static equilibrium can then be written as:

$$\mathbf{KU} = \mathbf{F} \tag{A.6}$$

where $\mathbf{U}$ is the global displacement vector and $\mathbf{F}$ is the global force vector. Once the displacements have been found the element strain vector $\boldsymbol{\epsilon}^{el}$ for layer l can be found in the global coordinate system as:

$$\boldsymbol{\epsilon}^{el} = \mathbf{B}^{el}\mathbf{U}^{e} \tag{A.7}$$

where $\mathbf{U}^{e}$ is the element displacement vector. To calculate maximum strain failure indices the strains are transformed to the material coordinate system and then divided by the allowable strain for each component.

The linearized buckling problem can be written as the following eigenvalue problem:

$$\left(\mathbf{K} + \lambda_j \mathbf{K}_\sigma\right) \boldsymbol{\Phi}_j = \mathbf{0}, \quad j = 1, 2, \ldots \tag{A.8}$$

where λ_j is the buckling load factor of mode j, described by the eigenvector $\boldsymbol{\Phi}_j$, and $\mathbf{K}_\sigma$ is the stress stiffness matrix. The stress stiffness matrix is found through an assembly of the element stress stiffness matrices given as:

$$\mathbf{K}_\sigma^e = \sum_{l=1}^{n_l} \int \left(\mathbf{G}_l^e\right)^T \mathbf{S}_l^e \mathbf{G}_l^e dV \tag{A.9}$$

where matrix $\mathbf{G}_l^e$ contains shape functions and shape function derivatives while matrix $\mathbf{S}_l^e$ contains layer stresses σ^{el}.

Design sensitivity analysis

The design sensitivity analysis is performed using the direct differentiation method. Thus, sensitivities of the displacement field for the static problem is obtained by differentiating the discretized finite element problem in (A.6) w.r.t. a thickness design variable t_{pl}, see e.g. Haftka and Gürdal (1992). The displacement sensitivities can thereby be found as:

$$\mathbf{K}\frac{d\mathbf{U}}{dt_{pl}} = -\frac{\partial \mathbf{K}}{\partial t_{pl}}\mathbf{D} + \frac{\partial \mathbf{F}}{\partial t_{pl}} \tag{A.10}$$

where the right-hand side is usually called the pseudo-load vector. The notation $d\mathbf{U}/dt_{pl}$ is used for the total derivative. In this work the loads are considered constant and hence the last term vanishes. The term $\frac{\partial \mathbf{K}}{\partial t_{pl}}\mathbf{U}$ is found through an assembly of element terms $\frac{\partial \mathbf{K}^e}{\partial t_{pl}}\mathbf{U}^e$. In this work the semi-analytical approach is used to find the partial derivative of the element stiffness matrix, i.e. it is evaluated through a second-order accurate central finite-difference:

$$\frac{\partial \mathbf{K}^e}{\partial t_{pl}} \approx \frac{\mathbf{K}^e(\mathbf{t} + \Delta t_{pl}) - \mathbf{K}^e(\mathbf{t} - \Delta t_{pl})}{2\Delta t_{pl}} \tag{A.11}$$

The perturbation Δt_{pl} is chosen as $t_{pl} \cdot 10^{-3}$. First order accurate forward difference approximations can also be applied in the semi-analytical approach, and no inaccuracy problems have been observed when using the faster first order approximations.

With solid-shell elements a change in thickness also involves a change in node coordinates. This is explained in the following section A.3.2.

Once the pseudo-load vector has been computed, then the displacement sensitivities $\frac{d\mathbf{D}}{dt_{pl}}$ in (A.10) can be determined efficiently by forward-backward substitution, re-using the already factored stiffness matrix $\mathbf{K}$ from (A.6). Sensitivities of failure indices are also found in a semi-analytical manner. Failure indices depend both explicitly on design variables and implicitly through displacements, $\mathrm{FI}_l^e = \mathrm{FI}_l^e(\mathbf{t}, \mathbf{U}^e(\mathbf{t}))$. The finite-difference approximation to the derivative can then be written:

$$\frac{d\mathrm{FI}^{el}}{dt_{pl}} \approx \frac{\mathrm{FI}^{el}(\mathbf{t} + \Delta t_{pl}, \mathbf{U}^e(\mathbf{t} + \Delta t_{pl})) - \mathrm{FI}^{el}(\mathbf{t} - \Delta t_{pl}, \mathbf{U}^e(\mathbf{t} - \Delta t_{pl}))}{2\Delta t_{pl}} \tag{A.12}$$

The previously found displacement sensitivities can be utilized to approximate the perturbed element displacements:

$$\mathbf{U}^e(\mathbf{t} + \Delta t_{pl}) \approx \mathbf{U}^e(\mathbf{t}) + \frac{d\mathbf{U}^e(\mathbf{t})}{dt_{pl}} \Delta t_{pl} \tag{A.13}$$

Linear buckling load factor sensitivities are treated in e.g. Lund (2009). For distinct eigenvalues the sensitivity can be written:

$$\frac{d\lambda_j}{dt_{pl}} = \mathbf{\Phi}_j^T \left(\frac{d\mathbf{K}}{dt_{pl}} + \lambda_j \frac{d\mathbf{K}_\sigma}{dt_{pl}} \right) \mathbf{\Phi}_j \tag{A.14}$$

assuming that $\mathbf{K}_\sigma$ have been ortho-normalized such that $\mathbf{\Phi}_j^T (-\mathbf{K}_\sigma) \mathbf{\Phi}_j = 1$. The derivative of the stiffness matrix have already been found in (A.11). The derivative of the element stress stiffness matrix is found in a semi-analytical manner similar to failure indices:

$$\frac{d\mathbf{K}_\sigma^e}{dt_{pl}} \approx \frac{\mathbf{K}_\sigma^e(\mathbf{t} + \Delta t_{pl}, \mathbf{U}^e(\mathbf{t} + \Delta t_{pl})) - \mathbf{K}_\sigma^e(\mathbf{t} - \Delta t_{pl}, \mathbf{U}^e(\mathbf{t} - \Delta t_{pl}))}{2\Delta t_{pl}} \tag{A.15}$$

and then (A.14) is computed based on the element terms.

Shape design sensitivity

As layered solid-shell elements are used, changing the thickness of a layer requires changing both the layup definition in the element, but also moving nodes. Thus the sizing optimization actually involves shape optimization. However, as opposed to the general case, node move directions are determined in advance. The distance the nodes are moved when changing a layer thickness is related to the mesh sensitivity, sometimes called the design velocity field (DVF). A simple 2D example demonstrating the implementation in this work is shown in Figure A.8. In the top figure the reference geometry is shown with three patches.

The first example is for the shear web (Patch 3), which is positioned according to its center line. If the thickness of a layer is increased with Δt_{pl} then nodes on each side of the center line should be moved with $\Delta t_{pl}/2$, and hence the movement of surface nodes compared to the layer thickness change is a factor of 0.5. When the thickness of

a layer in the shear web is increased nodes are moved in the directions of the arrows. Since a change in thickness in the shear web should not affect the thickness of Patch 1, not all directions are normal to the surface. Furthermore, in order to not distort the connecting element in Patch 1, some nodes not part of Patch 3 need to be moved as well. The next example is on Patch 1 which belongs to the outer shell. Here nodes are moved with reference to the outer geometry and only the internal nodes are moved with a factor of 1. The exception is the intermediate node between Patch 1 and Patch 2 which has a factor of 0.5. The factor of 0.5 is needed since the intermediate node is moved through changes to both Patch 1 and Patch 2. The move directions are normal to the surface except where connected to the shear web. Here move directions are tangential to the shear web in order not to affect the shear web thickness.

In practice this is implemented by having two factors and two directions defined for each node. The choice of direction/factor depends on if the patch is referenced as 'bottom' or 'mid'. The algorithm is used both for sensitivity analysis and for updating the design after each iteration. Care should be taken that thickness increases in the web do not collapse adjacent elements in the outer shell. This is prevented by having elements of sufficient size. Furthermore, a thickness error is introduced through the difference in angle between normal and non-normal directions. This error is proportional to the cosine of the angle difference and can be compensated with individual node factors, however this is not considered in this work due to relatively small angle differences.

A.3.3 Solution strategy

A sequential linear programming (SLP) strategy is utilized to solve the optimization problem. In the SLP approach, in each iteration, the equations are linearized with respect to design variables and linear programming (LP) is used to solve the problem. The linear programming problem is solved using CPLEX version 12.6, see ILOG IBM (2015). The solution approach is shown in the flow-chart in Figure A.9. The standard SLP approach is made more robust through a global convergence filter and adaptive move-limits.

The global convergence filter follows the description in Chin and Fletcher (2003), see also Sørensen and Lund (2015). With the global convergence filter, before a design change is accepted, a re-analysis is performed with updated design variables. The resulting objective function and the maximum infeasibility are recorded to a filter-list. The design change is accepted if either the objective function or the maximum constraint infeasibility is lower than previously recorded values. In this work a maximum allowable infeasibility of 1.5% is used. In practice this is done by initializing the global convergence filter to $(0.015, -1)$ for normalized maximum infeasibility and normalized objective function respectively. Since the normalized objective function can never be lower than -1, only designs with a maximum infeasibility lower than 1.5% can be accepted. If a design is not accepted, move-limits are reduced collectively and the linear programming problem is solved again.

Adaptive move-limits basically tighten move-limits for a given design variable if oscillating behavior is detected. The algorithm used for adaptive move-limits is described in Sørensen and Lund (2015). Initial move-limits are defined in terms of

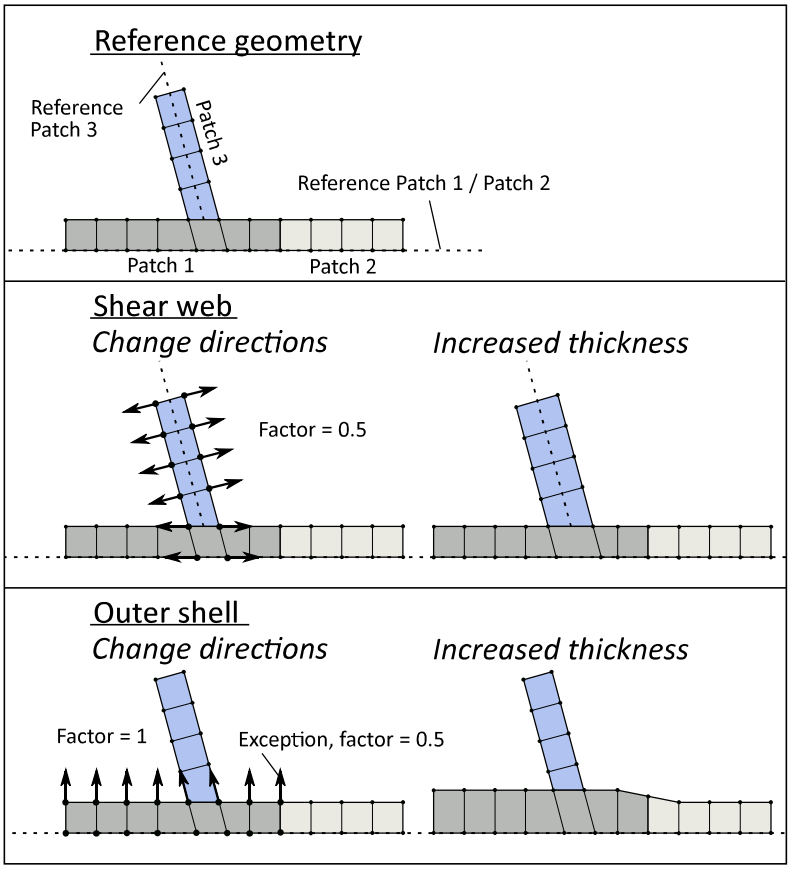

Fig. A.8: Method used for shape design sensitivities shown with two simple examples. The first example demonstrates how nodes in the shear web are moved, and the second how nodes in patches belonging to the outer shell are moved.

an allowable change in the D_{11} entry of the analytically calculated ABD matrix. The allowable change in D_{11} is here taken as 3%.

To ensure a feasible problem at all times a merit function approach, also called an elastic programming technique, is used. The merit function is inspired by the one used in Svanberg (1987). Here artificial design variables y_k are added to ensure that constraints are feasible. If there are K non-linear constraints, then constraint g_k can be written as:

$$\tilde{g}_k = g_k - y_k \leq g_k^{\max}, \quad k = 1, 2, \ldots, K \tag{A.16}$$

where y_k is the value needed to make the constraint feasible. Then a penalized objective function $\tilde{m}$ can be written as:

$$\tilde{m} = m + a \sum_{k}^{K} \left(c y_k + \frac{1}{2} y_k^2 \right) \tag{A.17}$$

where m is the real mass, and a and c are parameters. In this work $a = 1$ and $c = 1$ is used.

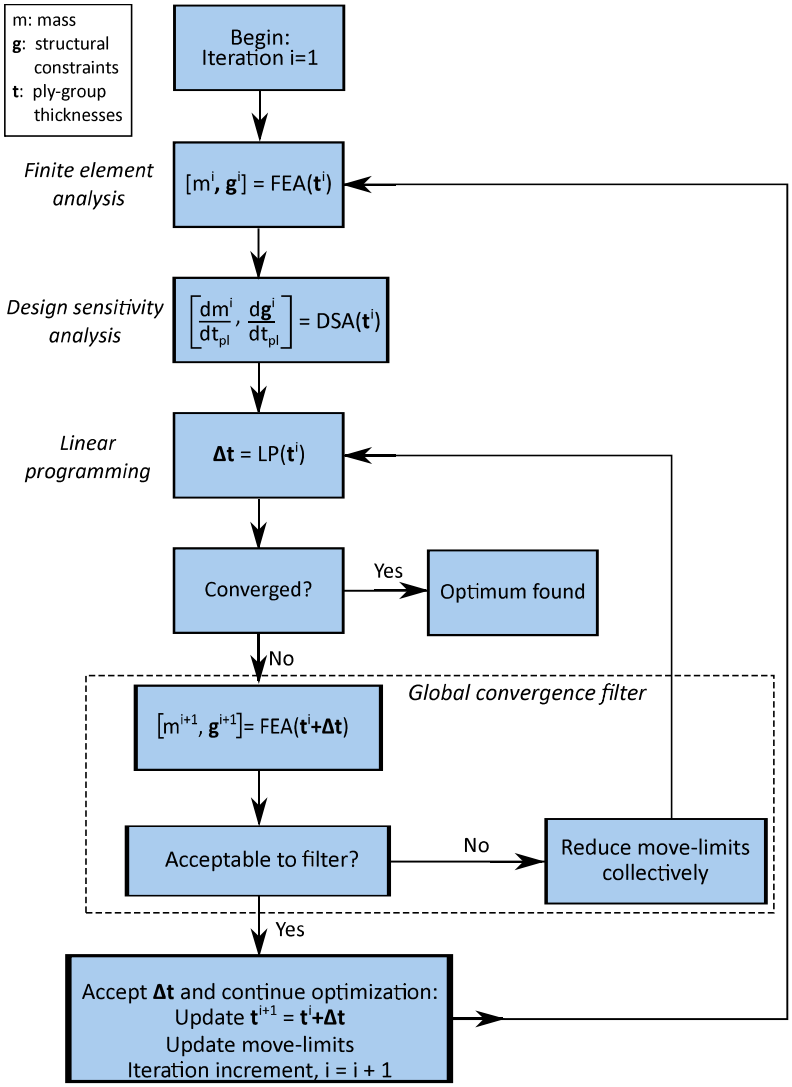

Fig. A.9: Flowchart of solution procedure.

A.3.4 Post-processing

The purpose of post-processing the optimized design is to obtain a manufacturable design. The post-processing is divided into three steps:

- Refinement of layup by interpolation
- Rounding to a discrete number of plies
- Avoiding multiple start/stops of the same ply

The first point is related to the longitudinal parameterization where the blade is divided into 2 m sections and a constant layup is used within the resulting patches. Due to this, ply-drop constraints can only be taken into account in an average sense. However, when manufacturing the blade only one ply-drop is allowed at a time. To circumvent this, the optimized thickness distribution is linearly interpolated with sampling points located at the center of each spanwise row of elements.

In the next step the interpolated distributions are rounded to a discrete number of layers. UD plies are in general not affected much by rounding due to relatively

thin plies of approximately 1 mm. Balsa layers on the other hand are more critical since they are assumed available only in plates of quarter inches. Due to this a simple rounding scheme (rounding to the closest number of plies) is used for the UD plies while balsa layers are rounded up if the continuous thickness corresponds to more than 10% of the balsa plate thickness.

The last step is related to avoiding multiple start/stops of the same ply. The ply-group concept with rounded thicknesses ensures manufacturability of the optimized design in the way that a ply-group can be placed in the mold one layer at a time with varying start/stop positions of that given layer. However, for a given ply it is not desirable to terminate it at one location only to start it again at a later position. Here this is referred to as local valleys and is dealt with simply by not dropping a ply if more plies of the same material/orientation are required at any point forward.

A.4 Results and Discussion

A.4.1 Convergence and criteria

The optimization history of the objective function and normalized constraints is shown in Figure A.10 with the post-processed results on the right side of the vertical dashed lines. Comparison of initial, optimized, and post-processed results are also listed in Table A.4. The mass is reduced from 30500 kg to 24185 kg and after post-processing the mass is 24556 kg as shown with the black line in Figure A.10a. This is a significant reduction in mass, however recall that the initial lay-up is achieved through a naive scaling of thicknesses to provide a feasible starting point, and that the thickness distributions in upwind and downwind sides are initially identical.

The normalized displacement constraint is also shown in Figure A.10a but with the right y-axis as reference. The displacement constraint can be seen to become active after 19 iterations. Once active it remains active for the remaining iterations. The post-processed results yield a slightly lower displacement of 18467 mm compared to 18518 mm for the optimized results.

Normalized buckling constraints are shown in Figure A.10b and it can be seen that buckling in LC12 is the first constraint to be active after 4 iterations. In later iterations buckling constraints in LC1, LC2, LC3, LC7 and LC8 also become active. Buckling load factors are slightly infeasible at times and are oscillating around the limit, but this is to be expected due to the linearizations used in SLP. After results are post-processed all buckling load factors are increased, improving the margin of safety.

Failure index constraints are shown in Figure A.10c. It can be seen that the failure index constraints in LC1 and LC2 eventually become active after 19 iterations while other load directions remain inactive. Note that it is the true maximum failure indices shown and not P-norm values. After post-processing maximum failure indices are reduced, again improving the margin of safety.

A.4.2 Ply-group distributions

The initial, optimized, and post-processed distributions of respectively UD and balsa ply-groups are shown in Figures A.11 and A.12. The thin horizontal lines correspond

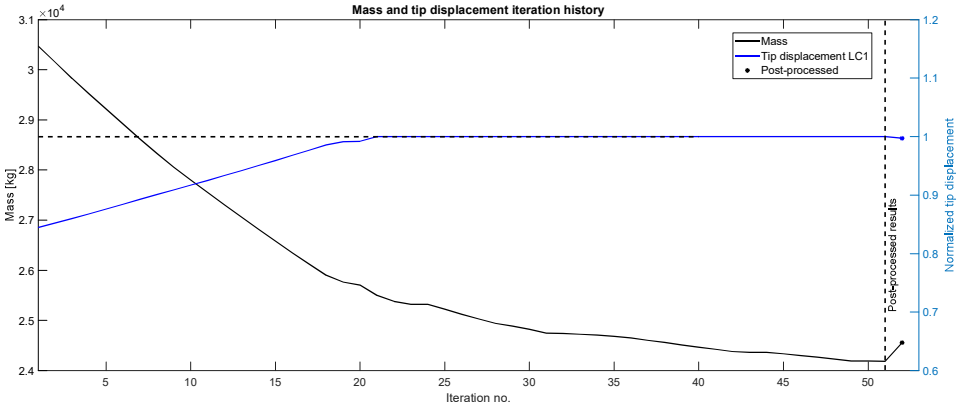

(a) Wind turbine blade mass is shown with the solid black line and has the left y-axis as reference. Normalized tip displacement in LC1 (flapwise deflection towards tower) is shown with the blue line with the right y-axis as reference. Displacement is normalized with respect to the allowable tip displacement of 18.5 m.

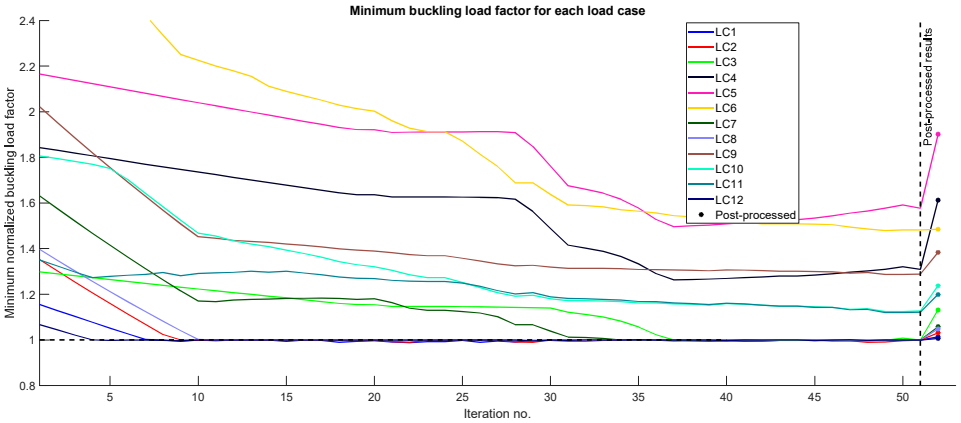

(b) Minimum normalized buckling load factors for each of the 12 load cases. Load factors are normalized with respect to the minimum allowable buckling load of 1.96.

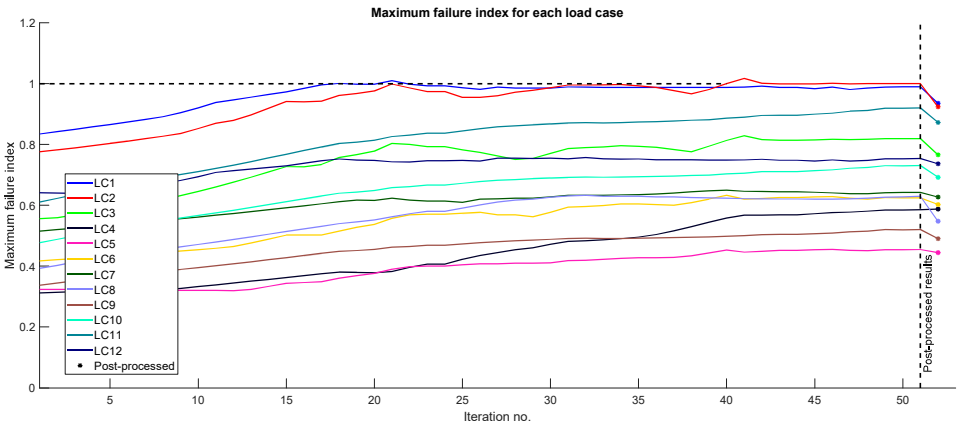

(c) Maximum failure index of whole blade for each of the 12 load cases.

Fig. A.10: Optimization history of objective and structural constraints during 51 iterations including post-processed results. In all cases the post-processed results are shown on the right-hand side of the figures.

Criteria	Load-case	Initial	Optimized	Post-processed	Limit
Mass (kg)	-	30470	24185	24556	-
Buckling load factor	LC1	2.26	1.96	1.99	≥ 1.96
Buckling load factor	LC2	2.65	1.96	2.02	≥ 1.96
Buckling load factor	LC3	2.55	1.96	2.22	≥ 1.96
Buckling load factor	LC4	3.62	2.57	3.17	≥ 1.96
Buckling load factor	LC5	4.25	3.09	3.73	≥ 1.96
Buckling load factor	LC6	7.64	2.91	2.91	≥ 1.96
Buckling load factor	LC7	3.20	1.96	2.07	≥ 1.96
Buckling load factor	LC8	2.74	1.96	2.06	≥ 1.96
Buckling load factor	LC9	3.97	2.53	2.71	≥ 1.96
Buckling load factor	LC10	3.54	2.21	2.43	≥ 1.96
Buckling load factor	LC11	2.65	2.20	2.35	≥ 1.96
Buckling load factor	LC12	2.09	1.96	1.98	≥ 1.96
Tip displacement (mm)	LC1	15652	18518	18467	≤ 18518
Failure index	LC1	0.83	0.98	0.93	≤ 1.00
Failure index	LC2	0.77	1.00	0.92	≤ 1.00
Failure index	LC3	0.55	0.81	0.76	≤ 1.00
Failure index	LC4	0.31	0.58	0.58	≤ 1.00
Failure index	LC5	0.32	0.45	0.44	≤ 1.00
Failure index	LC6	0.41	0.62	0.60	≤ 1.00
Failure index	LC7	0.51	0.64	0.62	≤ 1.00
Failure index	LC8	0.39	0.62	0.54	≤ 1.00
Failure index	LC9	0.33	0.52	0.49	≤ 1.00
Failure index	LC10	0.47	0.73	0.69	≤ 1.00
Failure index	LC11	0.61	0.92	0.87	≤ 1.00
Failure index	LC12	0.64	0.75	0.73	≤ 1.00

Table A.4: Comparison of objective and constraints between initial design, optimized design, and post-processed design.

to the ply-thickness of the ply-group material in question.

Furthermore, buckling and failure index results will be used to explain the thickness distributions obtained. Buckling mode shapes are visualized along paths placed in the center of each of the regions (TE DW, TEC DW, ect.). This is done for initial, optimized and post-processed layups for both LC1 and LC12 in Figures A.13 and A.14 respectively. In a similar way the maximum failure index in the downwind part of the main laminate in LC1 is shown in Figure A.15.

Root UD

The root UD ply-group is shown in Figure A.11a and is constrained to have a certain thickness at the root to provide space for bolt inserts. This ply-group is relatively costly since it spans the entire cross-section and much weight can be saved by reducing its thickness. The post-processed distribution is linearly extrapolated to the root-end. In practice it could be chosen to use a constant extrapolation to avoid short plies. A steep decrease corresponding to the maximum allowable thickness change is seen at 2 m. From 4-10 m the rate of thickness change is lower, and there is even a

small increase in thickness at 8 m. The post-processing removes the local valley and forms a plateau between 4-10 m. The small thickness increase at 8 m is likely required due to buckling mode 2 in LC1 located around this position, see Figure A.13c. Interestingly the buckling modes in LC1 near the root (mode 2, 6, and 7) disappear in the post-processed layup, see Figure A.13e. This is likely due to the 'filling' of local valleys, and the ceiling type rounding of the balsa.

Trailing edge UD and core

Distributions of the UD reinforcement in the trailing edge (TE UD) for downwind (DW) and upwind (UW) parts can be seen in Figures A.11b and A.11c respectively. More material is placed in the downwind part compared to the upwind part. This is expected since the largest flapwise loads (LC1, LC2, LC12) induce compressive loading in the downwind part making it more prone to failure due to both buckling and strength values that are lower for compression than tension. A rather steep increase in material can be seen at 30 m in Figure A.11b which coincides with the termination of the 3rd shear web. The thickness increase at 30 m seems to be needed to prevent buckling (mode 1 and 3) in LC12, see Figures A.14c and A.14d. Also with the initial layup buckling modes are prevalent in the trailing edge / trailing edge core from 30 m and onwards, see Figures A.13a and A.14a. This suggests that the 3rd shear web provides significant buckling resistance, and once terminated an increase in UD material is needed. On the upwind part of the TE UD a peak is seen at 10-12 m in Figure A.11c. This peak creates a local valley between 12-14 m which is avoided as part of the post-processing. The peak thickness may be due to buckling mode 2 in LC12, which can be seen in Figure A.14c. This mode is located around 12 m and partly excites the TE UW region though TE/TEC DW dominates.

Balsa in the trailing edge core (TEC) region is shown in Figures A.12a and A.12b for downwind (DW) and upwind (UW) parts respectively. Similar to the TE UD ply-group, an increase in thickness can be seen for the downwind side at 30 m to prevent buckling. In both the downwind and upwind part a thick balsa zone is seen around 12 m. For the downwind part this is probably again due to buckling mode 2 in LC12 which is located around 12 m, see Figure A.14c. For the upwind part the thickness increase at 12 m is found to match with the position of the 1st mode shape of the active buckling constraint in LC8. Furthermore, it makes sense for the optimizer to decrease the root UD ply-group around 12 m and instead reinforce the individual regions, especially as balsa is lighter than UD material. On the downwind part of TEC balsa the local valley between the peaks at 12 and 30 m is filled as part of the post-processing. This can be seen to eliminate the buckling modes 3 and 4 in LC1 which are located in this interval, see Figure A.13c vs. A.13e.

Main laminate

The main laminate (MA UD) for downwind (DW) and upwind (UW) can be seen in Figures A.11d and A.11e respectively. On the downwind part a slight overall thickness reduction can be seen, and the peak material thickness is moved spanwise from 32 m to 38 m. The peak at 38 m may be linked to buckling modes 6 and 7 in LC1 which can be seen to partly excite the MA DW region at this position. The maximum failure

index in the center of the MA DW region is shown in Figure A.15. Here the failure index can be seen to peak around 30 m. Note that the maximum failure index is not located exactly in the middle of the MA DW region, which is why the plotted failure index does not reach a value of 1. It is interesting to note that oscillations of approximately 2 m length of the failure index are seen for the initial and optimized layups. This corresponds to the 2 m longitudinal divisions. The post-processed layup yields a smoother failure index distribution, however the maximum values are not much different. On the upwind part more material is removed when compared to the downwind part, and the peak is kept at 32 m. For both upwind and downwind parts it can be seen that material is added between 10-14 m. This is similar to the thickness increase noted in the TEC region, and is needed to compensate for the thickness decrease in the root UD ply-group.

Leading edge laminate and core

The UD reinforcement in the leading edge (LE UD) is seen in Figure A.11f. The most material is removed in the inboard part of the blade. Here the leading edge region benefits from the root UD ply-group, and it seems little additional laminate reinforcement is needed. More laminate is needed between 24-50 m, and a uniform thickness is obtained from 50 m and beyond.

Balsa in the leading edge core (LEC) region is shown in Figures A.12c and A.12d. Similar to the TEC region the peak thickness of the downwind part is located at 14-16 m. From the load directions which have any active constraints it is only LC2 and LC3 which induce compression in the LEC region. It is found that buckling mode 5 in LC2 is located in the LEC region around 12-14 m with a buckling load factor of 1.97, and hence this is likely the reason for this reinforcement. For the upwind part more material is removed, and in both cases only 1-2 balsa plates are needed.

Shear webs

The thickness distribution of the shear webs is seen in Figure A.12e. A large overall reduction in thickness is found, and after post-processing the thickness is almost uniform. The shear web towards the trailing edge side can be seen in Figure A.13c to be part of buckling mode 2, 4, 6, and 7 in LC1. Furthermore, it is found that buckling in this shear web is governing for both LC2 and LC3.

Other observations

It is interesting to note that the buckling mode shapes of the initial layup are limited to rather specific areas of the blade, while the optimized buckling shapes in some cases span different regions across the entire length. This can be interpreted as a well distributed stiffness. With the optimized layup it can also be noted that some buckling load factors and mode shapes are very close, and may correspond to having multiple eigenvalues. The interaction between multiple eigenvalues is however not taken into account in the sensitivity analysis.

With regards to blade design it may be beneficial to either extend the 3rd shear web, or extend the width of the TEC balsa towards the trailing edge, in order to avoid

buckling in the TE/TEC region from 30 m and forward. With the optimized blade design buckling in this region is partly avoided through UD reinforcement in the TE region, which is a heavy solution compared to thicker balsa panels.

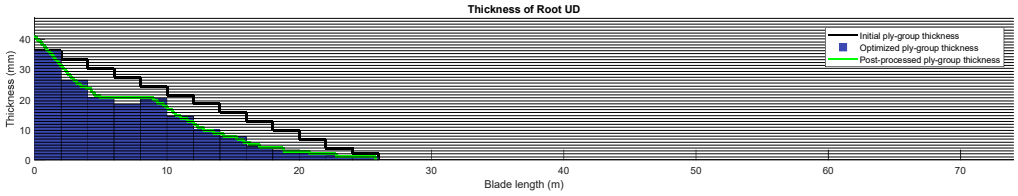

(a) Root UD ply-group (all-over).

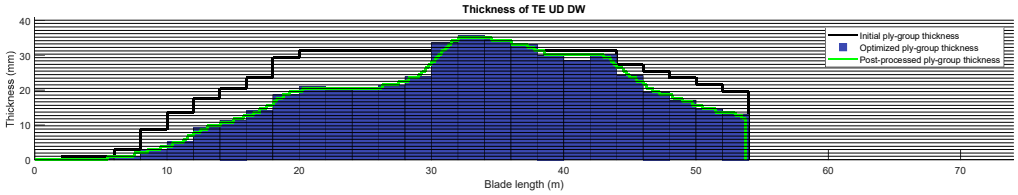

(b) Trailing edge UD downwind.

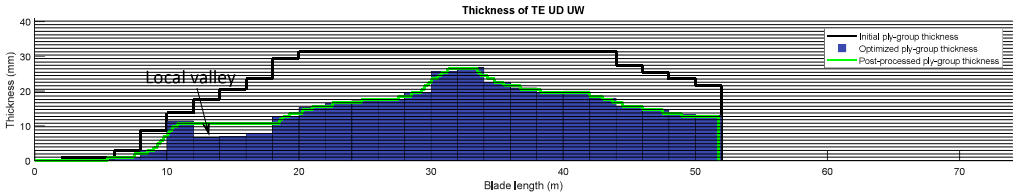

(c) Trailing edge UD upwind.

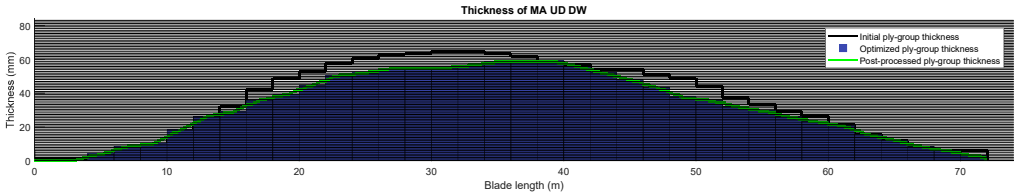

(d) Main laminate UD downwind.

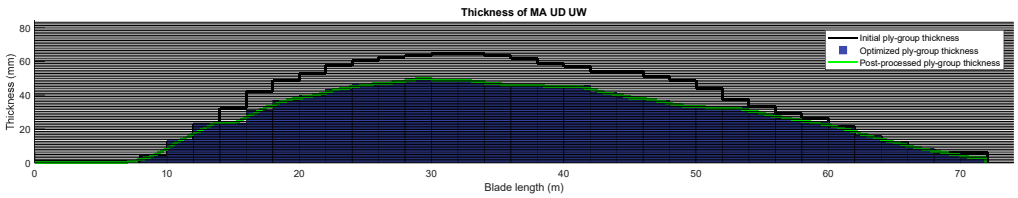

(e) Main laminate UD upwind.

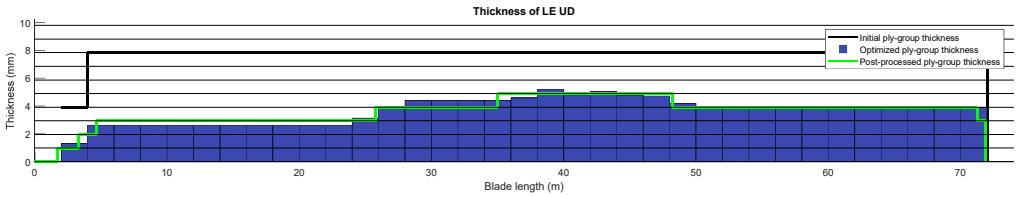

(f) Leading edge UD.

Fig. A.11: Optimized thickness distributions of UD ply-groups in respectively: root (uniform over cross-section), trailing edge, main laminate, and leading edge.

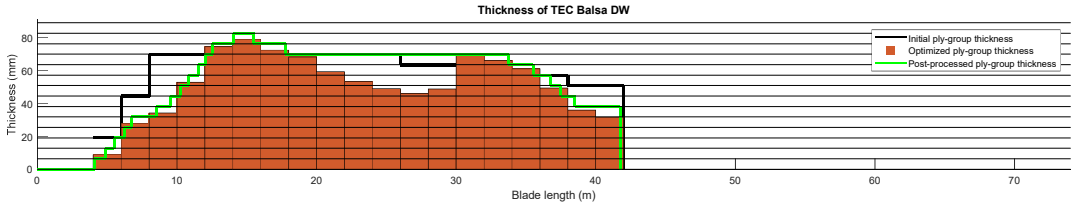

(a) Trailing edge core balsa downwind.

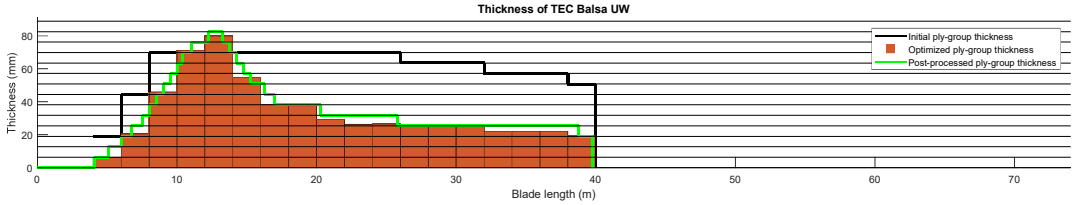

(b) Trailing edge core balsa upwind.

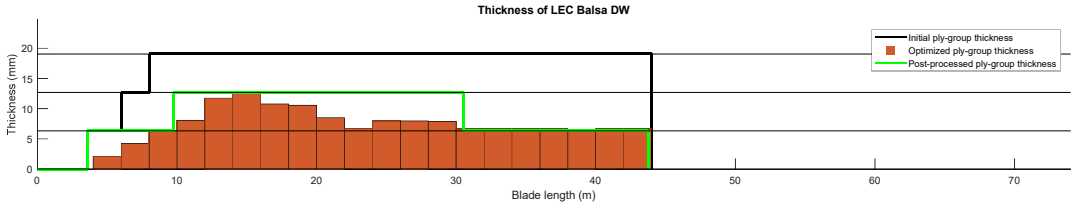

(c) Leading edge core balsa downwind.

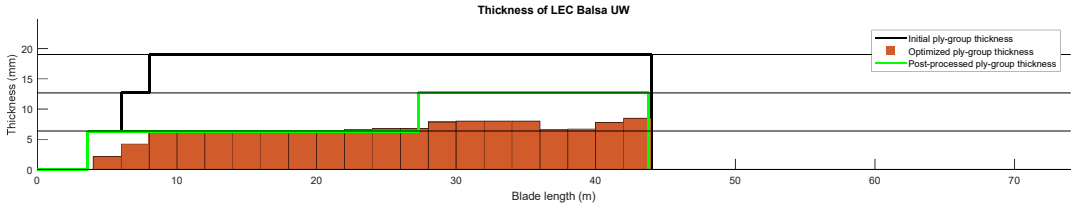

(d) Leading edge core balsa upwind.

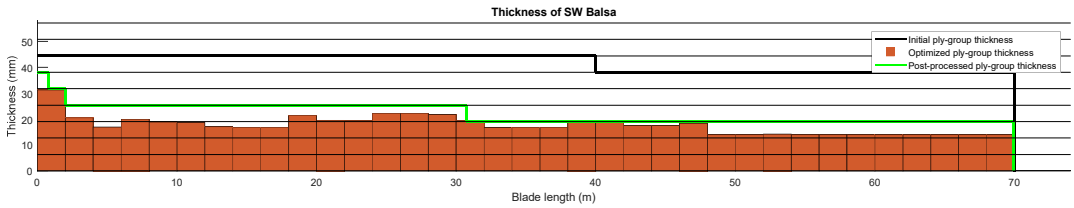

(e) Shear web balsa.

Fig. A.12: Optimized thickness distributions of balsa ply-groups in following regions: trailing edge core, leading edge core, and shear webs.

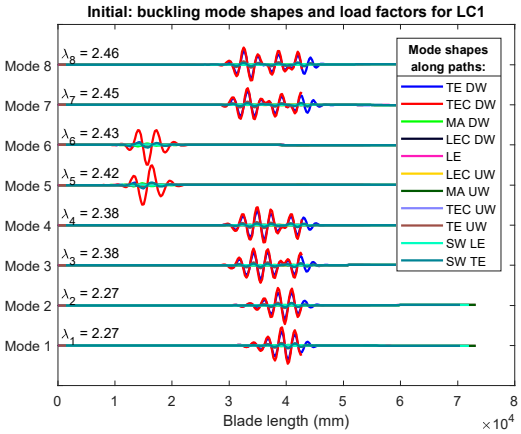

(a) Initial layup, LC1. The solid lines visualize mode shapes along the paths shown in (b). Buckling load factors (λ_j) are also shown.

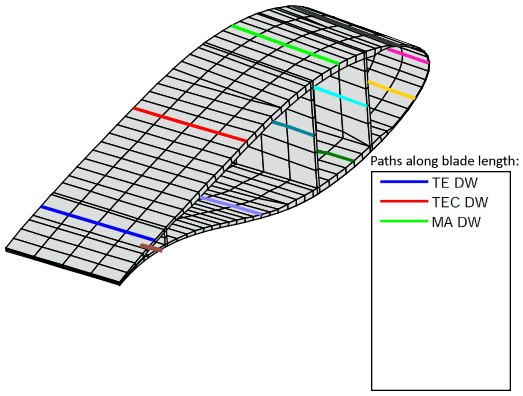

(b) Paths along the length of the blade used to show buckling mode shapes.

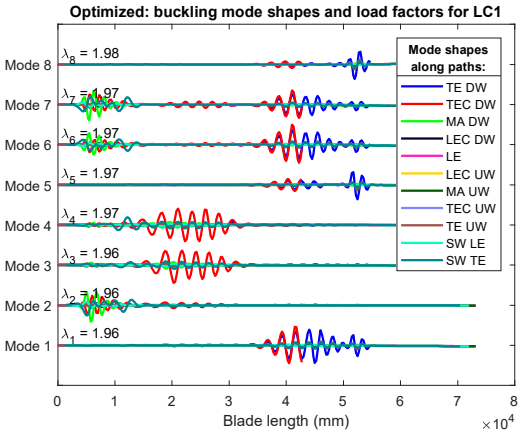

(c) Optimized layup, LC1. The solid lines visualize mode shapes along the paths shown in (b). Buckling load factors (λ_j) are also shown.

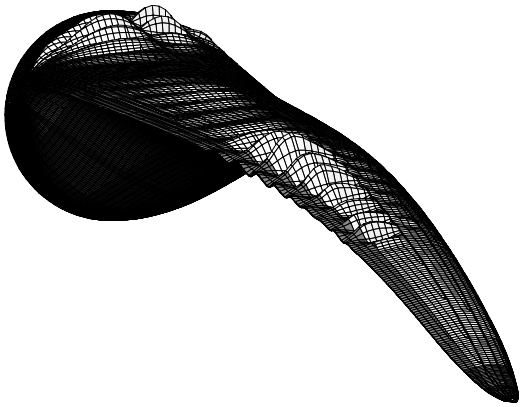

(d) Mode shape 6 of optimized layup in LC1. Display of a buckling mode that spans multiple regions and involves most of the blade length to some degree.

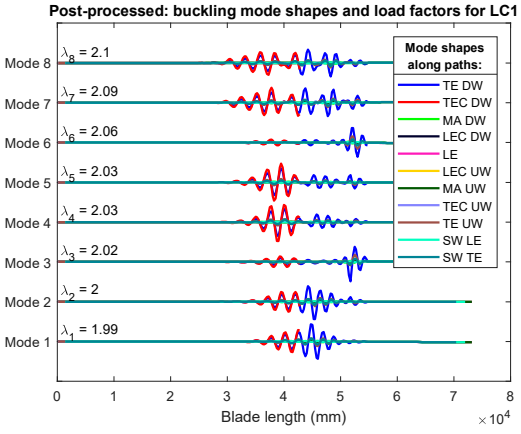

(e) Post-processed layup, LC1. The solid lines visualize mode shapes along the paths shown in (b). Buckling load factors (λ_j) are also shown.

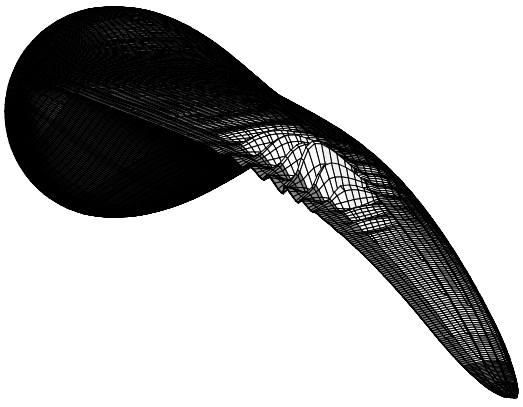

(f) Mode shape 1 of post-processed layup in LC1.

Fig. A.13: Comparison of LC1 buckling mode shapes and buckling load factors for initial, optimized, and post-processed lay-ups respectively. Buckling modes shapes are shown along paths located in the center of each of the regions (TE DW, TEC DW, etc.) as illustrated in subfigure b.

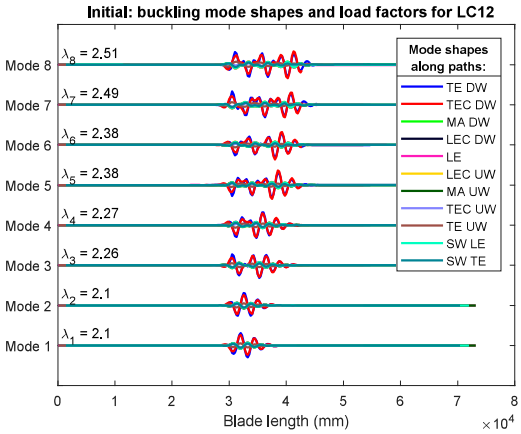

(a) Initial layup, LC12. The solid lines visualize mode shapes along the paths shown in (b). Buckling load factors (λ_j) are also shown.

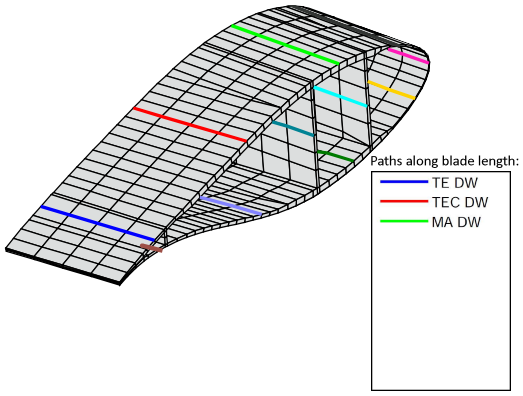

(b) Paths along the length of the blade used to show buckling mode shapes.

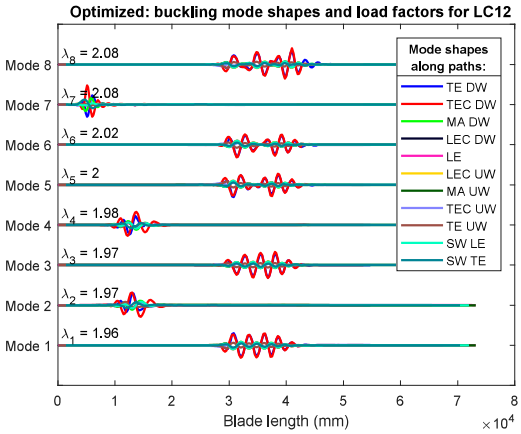

(c) Optimized layup, LC12. The solid lines visualize mode shapes along the paths shown in (b). Buckling load factors (λ_j) are also shown.

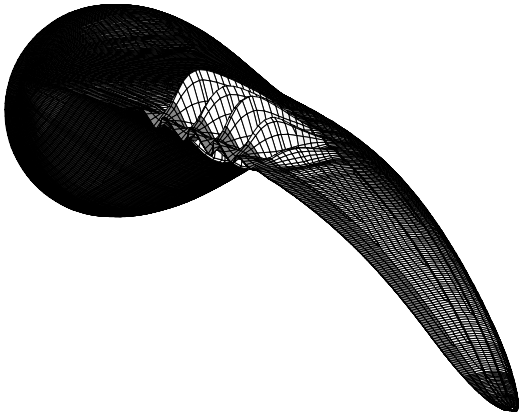

(d) Mode shape 1 of optimized layup in LC12. Critical buckling mode in the trailing edge/trailing edge core at 30 m where the 3rd shear web is terminated.

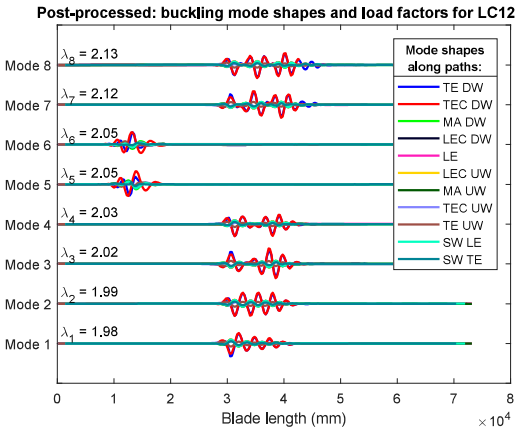

(e) Post-processed layup, LC12. The solid lines visualize mode shapes along the paths shown in (b). Buckling load factors (λ_j) are also shown.

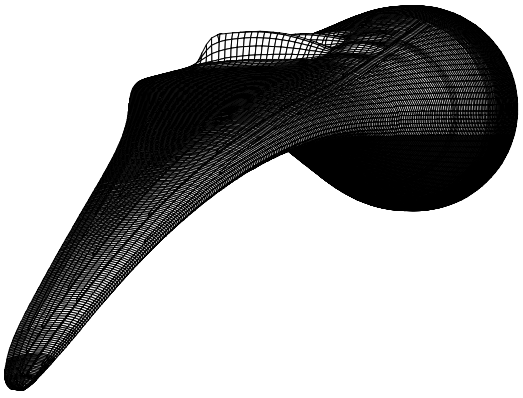

(f) Mode shape 5 of post-processed layup in LC12.

Fig. A.14: Comparison of LC12 buckling mode shapes and buckling load factors for initial, optimized, and post-processed lay-ups respectively. Buckling modes shapes are shown along paths located in the center of each of the regions (TE DW, TEC DW, etc.) as illustrated in subfigure b.

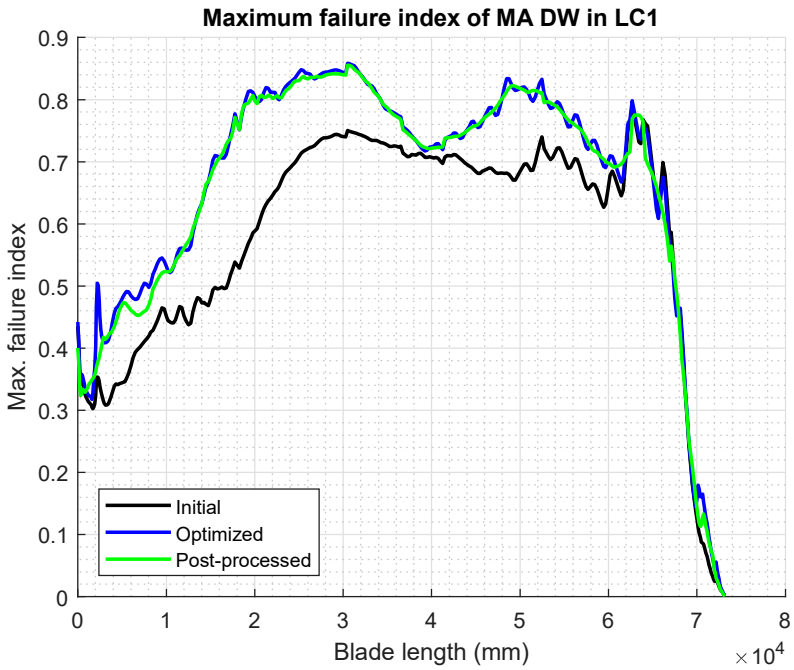

Fig. A.15: Max. failure index along the center of the downwind side main laminate in loadcase 1 shown for the initial, optimized, and post-processed layups respectively.

A.5 Limitations

A.5.1 Parameterization

The parameterization is suitable to structures that have characteristic regions with many contiguous plies of the same material/orientation. One of the main limitations is the predetermined sequence of ply-groups. The predetermined sequence is based on experience. For example, the main laminate region is expected to consist of mainly UD layers. However, in some regions it may make sense for the optimizer to choose another material for a given ply-group, and this is not possible. This could be overcome by adding ply-groups of other materials with a small starting thickness, and hence if beneficial the optimizer can increase the thickness of this ply-group. This would be at the expense of more design variables.

A.5.2 Modelling and non-linear analysis

The cross-section is divided into 10 characteristic regions with constant layup. The physical transitions between the regions are left out, however intermediate nodes are given the average thickness of its neighboring patches. This results in virtual transitions due to mesh compatibility rather than due to the physical transition. The transition between sandwich and monolithic sections could prove to be important in buckling of sandwich panels since the transitions essentially correspond to panel boundary conditions. A first order refinement could be achieved by adding intermediate transition patches with a layup corresponding to half the balsa in the center and half the monolithic layers on each side. This is left for future work.

The analysis approach using a full-scale solid-shell FE model does not have any inherent restrictions. Non-linear analysis is supported and could be used for all criteria on the expense of computational time. Recent work by Rosemeier et al. (2016) show that linear buckling analyses with the required partial safety factors are conservative, and probably a less conservative design could be achieved using non-linear FE. However, to reduce computational costs it may instead be beneficial to use linear analyses with experience-based partial factors and instead only use non-linear analyses for the verification of the final design. Partial safety factors could also be calibrated iteratively by non-linear analysis, similar to how Bottasso et al. (2014) calibrate the safety factors applied on a 2D FE cross-sectional model using a 3D FE model.

A.5.3 Extreme load envelope

In this work a provided extreme load envelope is used. This load envelope is assumed constant although the layup is changed meaning that the aero-elastic coupling is neglected. To circumvent this an aero-elastic re-analysis could be performed for e.g. every 10th structural optimization iteration. This is left for future work.

A.6 Conclusion

In this paper gradient based sizing of a modern wind turbine blade has been demonstrated. The demonstration takes offset in a full-scale 3D FE solid-shell model subject to an extreme load envelope of 12 load directions. A sequential linear programming (SLP) approach is used to minimize the mass of the blade while taking into account manufacturing constraints, tip displacement, buckling and static strength. In the optimization it is shown how solid-shell elements can be used for laminate sizing as changing a layer thickness involves moving nodes like in shape optimization.

The gradient based sizing optimization yields a mass reduction from 30470 kg to 24185 kg. However, in order to make the blade manufacturable the results are post-processed increasing the mass to 24556 kg while also increasing the margin of safety. Obtaining a manufacturable design through post-processing is possible due to the considered manufacturing constraints. Only two load directions result in active failure index constraints, while six load directions result in active buckling constraints, proving that including multiple load directions is essential. The parameterization of dividing the cross-section into 10 regions and the blade length into 2 m sections provides a coarse but sufficient patch discretization yielding relatively few design variables compared to the structure size. This in turn allows taking into account more load cases and constraints.

The parameterization with relatively few design variables and manufacturing constraints in combination with a gradient based approach enables a realistic sizing optimization of a modern 73.5 m offshore wind turbine blade. Utilizing a full-scale 3D FE solid-shell model in the optimization makes it possible to distribute the stiffness well resulting in many buckling modes on the limit across multiple load cases, and the obtained thickness distributions are found to match well with observed critical buckling modes.

Acknowledgements

This work was supported by the Innovation Fund Denmark project OPTI_MADE_BLADE, grant no. 75-2014-3. This support is gratefully acknowledged.

References

A. Albanesi, F. Bre, V. Fachinotti, and C. Gebhardt. Simultaneous ply-order, ply-number and ply-drop optimization of laminate wind turbine blades using the inverse finite element method. *Composite Structures*, 184:894–903, jan 2018. ISSN 0263-8223. doi: 10.1016/J.COMPSTRUCT.2017.10.051.

ANSYS Inc. ANSYS 18 Mechanical APDL Theory Reference. Technical report, ANSYS, Inc., Canonsburg, Pennsylvania, USA, 2017.

R. H. Barnes and E. V. Morozov. Structural optimisation of composite wind tur-

bine blade structures with variations of internal geometry configuration. *Composite Structures*, 152:158–167, 2016. ISSN 02638223. doi: 10.1016/j.compstruct.2016.05.013.

J. P. Blasques and M. Stolpe. Multi-material topology optimization of laminated composite beam cross sections. *Composite Structures*, 94(11):3278–3289, 2012. ISSN 02638223. doi: 10.1016/j.compstruct.2012.05.002.

C. L. Bottasso, F. Campagnolo, A. Croce, S. Dilli, F. Gualdoni, and M. B. Nielsen. Structural optimization of wind turbine rotor blades by multilevel sectional/multibody/3D-FEM analysis. *Multibody System Dynamics*, 32(1):87–116, 2014. ISSN 13845640. doi: 10.1007/s11044-013-9394-3.

K. Branner, P. Berring, C. Berggreen, and H. W. Knudsen. Torsional performance of wind turbine blades - Part II: Numerical validation. In *ICCM International Conferences on Composite Materials*, pages 1120–1121, 2007. ISBN 9784931136069.

N. Buckney, S. Green, A. Pirrera, and P. M. Weaver. On the structural topology of wind turbine blades. *Wind Energy*, 16(4):545–560, may 2013. ISSN 10954244. doi: 10.1002/we.1504.

J. Chen, Q. Wang, W. Z. Shen, X. Pang, S. Li, and X. Guo. Structural optimization study of composite wind turbine blade. *Materials & Design*, 46:247–255, 2013. ISSN 0261-3069. doi: https://doi.org/10.1016/j.matdes.2012.10.036.

C. M. Chin and R. Fletcher. On the global convergence of an SLP-filter algorithm that takes EQP steps. *Mathematical Programming, Series B*, 96(1):161–177, 2003. ISSN 00255610. doi: 10.1007/s10107-003-0378-6.

Dassault Systèmes. Abaqus 2017 Theory Manual. Technical report, Dassault Systèmes Simulia Corp., Providence, Rhode Island, USA, 2017.

DNV-GL. DNVGL-ST-0376 Rotor blades for wind turbines. Technical Report December, DNV GL Group AS, Oslo, Norway, 2015.

GL. Rules and Guidelines – IV Industrial Services –Part 1: Guideline for the Certification of Wind Turbines. Technical report, Germanischer Lloyd Industrial Services, Hamburg, Germany, 2010.

R. T. Haftka and Z. Gürdal. *Elements of structural optimization*. Kluwer Academic Publishers, 1992. ISBN 978-0-7923-1505-6.

P. U. Haselbach. An advanced structural trailing edge modelling method for wind turbine blades. *Composite Structures*, 180:521–530, nov 2017. ISSN 02638223. doi: 10.1016/j.compstruct.2017.08.029.

IEC. IEC 61400-1:2005. Technical report, International Electrotechnical Commission, Genève, Schweiz, jan 2005.

ILOG IBM. IBM ILOG CPLEX Optimization Studio, 2015.

L. Johansen and E. Lund. Optimization of laminated composite structures using delamination criteria and hierarchical models. *Structural and Multidisciplinary Optimization*, 38(4):357–375, 2009. ISSN 1615147X. doi: 10.1007/s00158-008-0280-1.

M. Jureczko, M. Pawlak, and A. Mężyk. Optimisation of wind turbine blades. *Journal of Materials Processing Technology*, 167(2-3):463–471, 2005. ISSN 09240136. doi: 10.1016/j.jmatprotec.2005.06.055.

D. L. Laird, F. C. Montoya, and D. J. Malcolm. Finite element modeling of wind turbine blades. In *Collection of the 2005 ASME Wind Energy Symposium Technical Papers at the 43rd AIAA Aerospace Sciences Meeting and Exhibit*, pages 9–17, 2005. ISBN 1563477262.

E. Lund. Buckling topology optimization of laminated multi-material composite shell structures. *Composite Structures*, 91(2):158–167, 2009. ISSN 02638223. doi: 10.1016/j.compstruct.2009.04.046.

E. Lund. Discrete Material and Thickness Optimization of laminated composite structures including failure criteria. *Structural and Multidisciplinary Optimization*, 57(6):2357–2375, dec 2018. ISSN 1615-147X. doi: 10.1007/s00158-017-1866-2.

MUST. The MUltidisciplinary Synthesis Tool (MUST), Department of Materials and Production, Aalborg University, 2018.

J. Oest and E. Lund. Topology optimization with finite-life fatigue constraints. *Structural and Multidisciplinary Optimization*, 56(5):1045–1059, nov 2017. ISSN 1615-147X. doi: 10.1007/s00158-017-1701-9.

M. Rosemeier, P. Berring, and K. Branner. Non-linear ultimate strength and stability limit state analysis of a wind turbine blade. *Wind Energy*, 19(5):825–846, may 2016. ISSN 10954244. doi: 10.1002/we.1868.

R. Sørensen and E. Lund. Thickness filters for gradient based multi-material and thickness optimization of laminated composite structures. *Structural and Multidisciplinary Optimization*, 52(2):227–250, 2015. ISSN 16151488. doi: 10.1007/s00158-015-1230-3.

S. N. Sørensen, R. Sørensen, and E. Lund. DMTO – a method for Discrete Material and Thickness Optimization of laminated composite structures. *Structural and Multidisciplinary Optimization*, 50(1):25–47, jul 2014. ISSN 1615-147X. doi: 10.1007/s00158-014-1047-5.

K. Svanberg. The method of moving asymptotes—a new method for structural optimization. *International Journal for Numerical Methods in Engineering*, 24(2):359–373, feb 1987. ISSN 0029-5981. doi: 10.1002/nme.1620240207.